Laser processing of gallium nitride–based light-emitting diodes with ultraviolet picosecond laser pulses

Rüdiger Moser
Michael Kunzer
Christian Goßler
Klaus Köhler
Wilfried Pletschen
Fraunhofer-Institut für Angewandte Festkörperphysik
Tullastrasse 72
D-79108 Freiburg, Germany
E-mail: ruediger.moser@iaf.fraunhofer.de

Ulrich T. Schwarz
Fraunhofer-Institut für Angewandte Festkörperphysik
Tullastrasse 72
D-79108 Freiburg, Germany
and
University of Freiburg
Institute of Microsystems Engineering
Laboratory for Optoelectronics
Georges-Köhler-Allee 103
79110 Freiburg, Germany

Joachim Wagner
Fraunhofer-Institut für Angewandte Festkörperphysik
Tullastrasse 72
D-79108 Freiburg, Germany

Abstract. The fabrication of optoelectronic devices such as light-emitting diodes (LEDs) typically involves photolithography steps, requiring specific lithography masks. This approach is expensive, inflexible and time consuming, in particular for prototyping. Therefore it would be attractive to replace these steps by direct writing techniques such as laser processing, which would speed up, for example the development and prototyping of new devices. Picosecond lasers provide a universal tool for material processing. Due to the short pulse length, material is removed by a process called "cold ablation," with minimal thermal damage to neighboring regions. As a result, better-defined structures with smoother and cleaner side walls can be fabricated compared to nanosecond-pulsed laser-based processing. We report on fully laser-processed planar gallium nitride-based LEDs fabricated using only ps laser processing for pattern definition and material removal. On the bare semiconductor wafer, isolation trenches and mesa structures are formed directly by ultraviolet ps laser pulse writing. For the direct deposition of patterned ohmic contact metallizations, the ps laser fabrication and subsequent use of high-resolution shadow masks is presented. Finally, the ps laser-processed LEDs are electrically and optically characterized and their characteristics compared with those of conventionally fabricated mesa LEDs. [DOI: 10.1117/1.OE.51.11.114301]

Subject terms: gallium nitride light-emitting diode; prototyping; ultraviolet; picosecond laser; direct writing; ablation threshold; trench; mesa.

Paper 121144P received Aug. 9, 2012; revised manuscript received Oct. 23, 2012; accepted for publication Oct. 23, 2012; published online Nov. 13, 2012.

1 Introduction

During recent years, considerable effort has been directed toward research and development of new laser material processing techniques. As state-of-the-art lasers provide high output power and high repetition rates, laser processing finds increasing use in industrial applications.[1,2] Most of the laser processes used for welding, drilling, or ablating material work with nanosecond laser pulses or in continuous wave (CW) operation. Recently, picosecond lasers have become sufficiently mature for daily operation in industrial environments. Therefore research focuses on ultra-short pulse laser processing, among others. Due to the short pulse, a higher peak power is available than for ns lasers. Therefore the processing of transparent materials having a band gap larger than the photon energy of the laser becomes possible via nonlinear optical and multi-photon absorption processes.[3,4]

Besides processing of transparent materials, ultra-short laser pulses exhibit another important feature. Light–matter interaction occurs via absorption of the laser energy by free electrons due to the inverse Bremsstrahlung, followed by their thermalization within the electron subsystem, electron to lattice heat transfer, and energy loss due to electron heat transport within the target.[5] When talking about ultra-short laser pulses, the time constants for the different mechanisms are important. It has been shown that in the case of metals, the typical time scale for the fast electron cooling and the energy transfer to the lattice is of the order of 1 ps. In the case of laser pulses with duration of a few picoseconds, the lattice temperature remains well below the electron temperature.[5] As a result, melting in the region around the ablated area is drastically reduced compared to nanosecond pulses. Therefore better defined structures with smoother and cleaner sidewalls can be fabricated.

In industrial production, the processing of metals is often the main focus. But ps laser processing is also attractive for cost-effective fabrication of semiconductor devices, such as solar cells. Recently, research has focused on the development of laser processing steps for thin-film solar cells, e.g., the monolithic serial interconnection, where thin layers have to be selectively removed.[6–8] But laser processing is also interesting for other optoelectronic devices such as light-emitting diodes (LEDs). A major advantage of laser processing is its capability for rapid prototyping of new devices, as it can be used as a direct writing technique. The conventional way to fabricate LEDs is the use of photolithography for contact and mesa definition and etching techniques for material removal. Each processing step requires a separate lithography mask. The fabrication of lithography masks is in general a significant cost factor and time-consuming, which is in particular unfavorable when addressing prototype fabrication or small-volume production. Therefore it is attractive to replace

0091-3286/2012/$25.00 © 2012 SPIE

these lithography steps by direct writing techniques such as laser processing.

There are two fundamental possibilities to implement laser processing. First, a photoresist can be exposed by direct laser writing, eliminating the need for a lithography mask, followed by an etching or lift-off process, similar to standard photolithography-based processing. Second, the material removal can be carried out directly by laser processing, also known as laser etching. The latter process is used in this work, demonstrating direct laser processing of gallium nitride (GaN)-based LEDs with ultraviolet picosecond laser pulses.

2 Experimental Setup

2.1 *Laser Micromachining System*

The laser processing is carried out by a purpose-built laser-micromachining system. A schematic drawing of the system is shown in Fig. 1. A ps laser system (Lumera, Super Rapid) is used as an irradiation source with three different wavelengths available (355, 532, and 1064 nm), a pulse length of ≈10 ps, variable repetition rate between 80 and 1000 kHz, and the option to generate pulses on demand. For the present study, a laser wavelength of 355 nm was used for all experiments. The linearly polarized output beam has a beam quality factor of $M^2 \approx 1.1$. The maximum pulse energy at 355 nm is 35 μJ. An internal half-waveplate combined with a polarizing beam splitter allows continuous tuning of the output power between zero and maximum power.

The whole system is designed to achieve a very high mechanical precision. Hence fixed optics are used instead of scanning optics such as a galvo-scanner. The laser-micromachining system comprises two beam paths, one consisting of a 4× beam expander to widen and collimate the beam, followed by a triplet lens with a focal length of 25 mm to focus the beam to a $1/e^2$ diameter of 1.7 μm. The second beam path contains just a single aspheric focus lens with a focal distance of 30 mm, resulting in a $1/e^2$ diameter of 7 μm. Each focusing optic is mounted on a linear translation stage to control the vertical focus position (z-axis). The laser beam can be switched between the two paths with the help of a movable mirror. Both beam paths are optimized for a wavelength of 355 nm. The wafer is placed on a vacuum chuck mounted on a high-precision air-bearing wafer stage. The stage exhibits a very high position reproducibility of 200 nm and has a maximum travel speed of 100 mm/s. Furthermore, the mechanical translation system allows a trigger output at fixed user-defined positions when scanning a contour, for example. This option, called position-synchronized output (PSO), is used to trigger an electro-optical modulator in the laser system to select single pulses out of the pulse train (pulse on demand). Hence it is possible to freely adjust the distance between the individual laser pulses [inter-pulse distance (IPD)], independent of the scanning speed of the stage. In this mode, the effective repetition rate therefore depends on the IPD.

The laser-micromachining system also comprises two different microscopes for inspection and precise alignment of the samples. To adjust the focus position with respect to the sample surface, a high-precision optical distance sensor is used to measure the height of the sample. All of the components are mounted on a granite gantry and are enclosed by laser safety housing. A filter and flow unit is used for forced air circulation to protect the optics and the samples from dust. Laser processing is carried out under a nitrogen inert gas atmosphere. The repetition rate of the laser was set to 100 kHz. The IPD was defined using the PSO option.

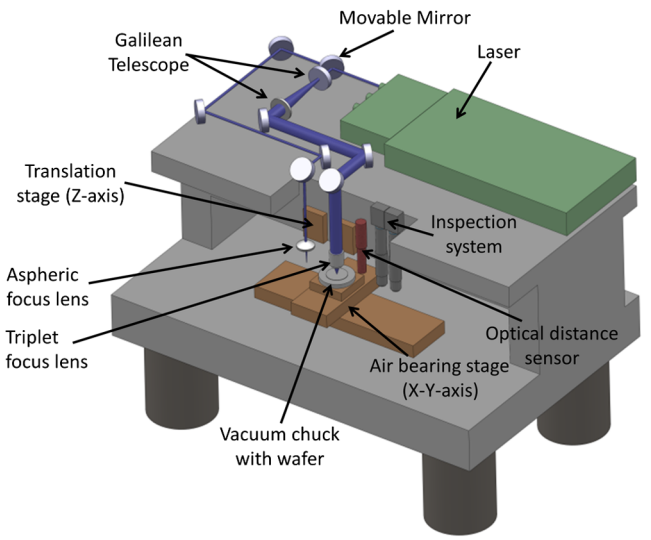

Fig. 1 Schematic drawing of the purpose-built ps laser-micromachining system used for the processing of GaN-based LEDs. The whole system is enclosed by laser safety housing not shown in the drawing.

2.2 *LED Wafers*

The LED structures were grown on 2-inch single-side polished (0001) sapphire wafers by metalorganic vapor-phase epitaxy (MOVPE) in a single wafer reactor (Aixtron AIX 200/RF). A schematic diagram of the LED structure is shown in Fig. 2. From bottom to top, the layer sequences are as follows: a GaN nucleation layer followed by a thick GaN buffer layer and a 1 μm thick Si doped n-GaN layer, then three InGaN quantum wells grown embedded between GaN barrier layers. To prevent electron recombination in the top p-doped GaN:Mg layer, a Mg doped p-AlGaN electron blocking layer (EBL) is inserted. The total thickness of the epitaxial layer stack is around 4 μm. The composition of the quantum wells is designed for an emission wavelength of 400 nm.

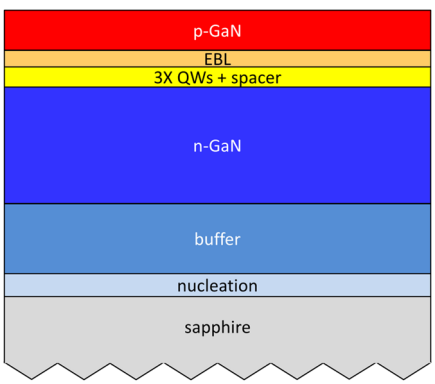

Fig. 2 Schematic diagram of the LED structure used for the laser processing. The design wavelength of the structure is 400 nm.

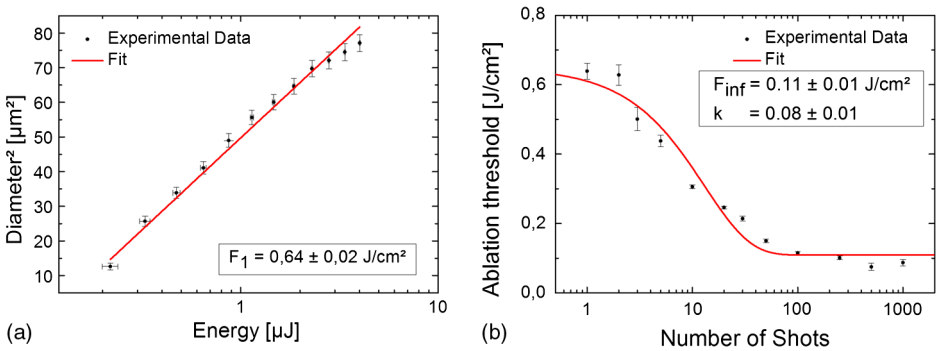

Fig. 3 (a) Crater diameter vs. pulse energy for single-pulse irradiation of the III-N layer sequence. The experimental data were obtained using a focus diameter of 7 μm. (b) Ablation threshold vs. the number of irradiation pulses. Due to incubation effects, the ablation threshold is reduced significantly.

3 Ablation Threshold

When performing laser material processing, and especially the removal of material by ablation up to a well-defined depth, the knowledge of the ablation threshold of the corresponding materials is essential. The ablation threshold depends not only on the material, but also on the laser pulse length, the laser wavelength, and the number of subsequent pulses applied to the same position on the surface. Because the laser beam of the micromachining system has a Gaussian beam profile, the diameter of the ablation crater formed depends on the pulse energy in the following way:[9]

$$d^2 = 2\omega_0^2 \ln\left[\frac{2E_P}{F_1 \pi \omega_0^2}\right], \tag{1}$$

where d denotes the crater diameter, ω_0 the $1/e^2$ diameter of the focus, E_P the pulse energy, and F_1 the material-dependent threshold fluence for ablation. When applying single laser pulses with varying pulse energy onto the sample surface, the resulting crater diameter can be plotted against the pulse energy used. By fitting the data with Eq. (1), the ablation threshold can be determined by using ω_0 and F_1 as fit parameters. Such measurements were carried out using the 7 μm focus diameter. Figure 3(a) shows the result obtained for the III-N LED-layer sequence grown on the sapphire substrate. The ablation threshold for single-pulse irradiation is $F_1 = 0.64 \pm 0.02$ J/cm^2.

When fabricating a trench, for example, a certain pulse overlap is necessary to realize smooth sidewalls and a flat bottom. Therefore the same position is irradiated several times. Owing to incubation effects, the ablation threshold decreases significantly when increasing the number of pulses applied. In the case of femtosecond (fs) pulses, this has been attributed to laser-induced defect formation,[10] and the dependence of the ablation threshold on the number of applied laser pulses can be expressed in the following way:

$$F_{\mathrm{th}}(N) = F_{\mathrm{inf}} + [F_1 - F_{\mathrm{inf}}] \exp[-k(N-1)], \tag{2}$$

where $F_{\mathrm{th}}(N)$ is the ablation threshold depending on the number of laser shots N, F_{inf} is the ablation threshold for an infinity number of shots, F_1 again the ablation threshold for single-pulse irradiation, and k an empirical parameter characterizing the strength of defect accumulation. Figure 3(b) shows the ablation threshold vs. the number of pulses applied to the surface for the III-N LED-layer sequence. The effective repetition rate was set to 50 kHz by using the pulse-on-demand option of the laser system. As reported in the literature, thermal accumulation effects are avoided in the case of sapphire if repetition rates smaller than 500 kHz are used.[11] Because GaN exhibits a very high thermal diffusivity, which is around a factor of 6.5 larger compared to sapphire ($D_{\mathrm{sapphire}} = 15 \cdot 10^{-6}$ m^2/s, $D_{\mathrm{GaN}} = 98.6 \cdot 10^{-6}$ m^2/s),[12] thermal accumulation should also be avoided. The experimental data can be well described using Eq. (2). As can be seen, the ablation threshold decreases with the increasing number of irradiation pulses, reaching a constant level at a very large number of shots (>100). The same investigations were also performed for sapphire. The results for the single-pulse irradiation and for the limiting case of an infinite number of irradiating pulses are given in Table 1.

Table 1 Ablation threshold of the III-N LED layer sequence and sapphire for a laser wavelength of 355 nm and a pulse duration of 10 ps.

	III-N LED layer	Sapphire
Single-pulse irradiation (J/cm^2)	0.65 ± 0.02	5.8 ± 0.2
∞-pulse irradiation (J/cm^2)	0.11 ± 0.01	0.8 ± 0.2
k	0.08 ± 0.01	0.07 ± 0.01

When comparing the ablation threshold for single pulse irradiation, the value for sapphire is a factor of 9 larger than that for the LED structure. In the case of ns laser pulses at 355 nm, an even larger difference of a factor of 18 was reported.[13] When comparing the values for an infinite number of laser pulses, the difference in ablation threshold is reduced, but is still around a factor of 7. In the case of material processing of the III-N layer sequence, the sapphire remains undamaged as long as the fluence is below $F_{\mathrm{inf}} = 0.8$ J/cm^2.

4 Device Processing

To obtain a working LED, a series of processing steps is required. A schematic diagram of the four fundamental processing steps is shown in Fig. 4, displaying the LED layer sequence as just a simple p–n diode for clarity of presentation. The first processing step consists of the patterned deposition of ohmic metal p-contacts onto the p-GaN. Second, a mesa structure is generated, to electrically isolate the

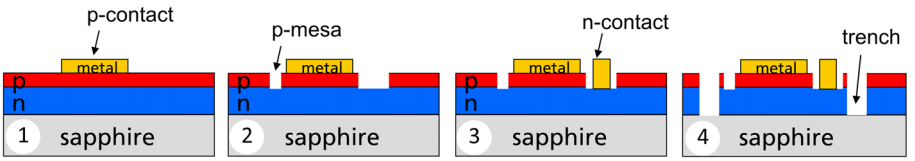

Fig. 4 Four fundamental processing steps for the realization of a functional LED device. For none of these steps lithography is used. For simplicity only the important LED layers are shown.

individual LEDs and expose the n-GaN for the subsequent deposition of the ohmic n-contacts. Third, the n-contacts are deposited onto the exposed areas. Finally, the individual LED chips are fully isolated against each other by fabricating trenches through the epitaxial layers down to the sapphire substrate. In standard LED fabrication technology, photolithography in combination with resist etching and lift-off masks are used for dry etching and contact metal deposition. In the present study, for all of these fabrication steps, alternative processing recipes have been developed that do not resort photolithography and associated costly and time-consuming lithography mask fabrication. Because the laser-micromachining system contains no scanning optics, and processing speed was not optimized for the presented investigations, the patterning of the LED layer sequence took several hours, strongly depending on the layout of the LED wafer. By implementing scanning optics, processing speed can be enhanced by more than an order of magnitude.

4.1 *High-Resolution Shadow Masks for the Deposition of Ohmic Contacts*

For the deposition of ohmic contacts, for example, the patterned deposition of metal layer sequences is necessary. For this purpose, high-resolution shadow masks are fabricated using the laser-micromachining system. A molybdenum foil with a thickness of 30 μm is used as raw material. For mask fabrication, the beam path comprising the aspheric focus lens ($\omega_0 = 7$ μm) was used, since it offers a larger focus depth compared to the triplet focusing lens. The IPD was set to 0.3 μm and a pulse energy of 10 μJ was used, optimized for smooth sidewalls. To cut out the intended mask structure, each laser trace was repeated 10 times to obtain smooth and clean sidewalls.

Figure 5(a) shows an image of a ps ultraviolet (UV) laser micro-machined shadow mask, 2 inches in diameter, containing a sequence of test structures. The detailed view shows a microscope image taken in transmission mode. The cut-out parts of the foil appear bright, whereas the remaining parts stay black. The narrowest bridging section on the bottom right has a width of 10 μm. In Fig. 5(b), a comparison of two nominally identical shadow masks is shown. The mask on the lefthand side was fabricated with an ns-pulse laser machining system at a wavelength of 1064 nm, whereas the mask on the righthand side was fabricated with the ps laser-micromachining system described above. It can be clearly seen that for the mask fabricated with the ps laser system, the sidewall roughness is significantly reduced compared to ns-pulse laser micro-fabrication, and the individual features are thus much better defined. One important reason for the improvement is the considerably reduced heat-affected zone around the area directly hit by the laser due to the short laser pulses as discussed above.

The patterned shadow mask is then placed on top of the LED wafer and the stack is inserted into a vacuum evaporation system for the deposition of the ohmic p-contact metallization. The Ni/Au metallization sequence is deposited onto the LED wafer only in the openings of the shadow mask. After mask removal, the contacts are annealed. A diagram of this processing step is shown in Fig. 6(a). Figure 6(b) shows a photograph of an LED wafer with metal contacts deposited on top of the p-GaN layer by shadow mask evaporation. The detailed view in Fig. 6(b) shows microscope images of different Ni/Au contact pads with different geometries showing smooth and clean sidewalls.

Because the layer thickness of typical contact metallizations is between 300 and 400 nm, only thin layers are evaporated onto the shadow masks. Therefore the masks can be used multiple times, as long as the evaporated layers do not peel off. The mask shown in Fig. 5(a) was successfully used up to 100 times.

4.2 *p-Mesa Definition*

After the deposition of the p-contact, the next processing step is the patterning of the epitaxial layer sequence. To achieve a well-defined electrically injected device area as well as

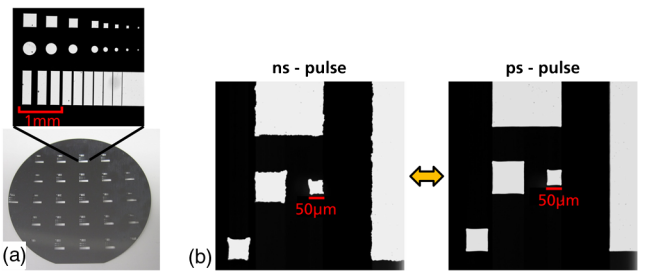

Fig. 5 (a) Two-inch shadow mask containing test structures fabricated by pulsed ps UV laser micromachining. The narrowest bridging section in the detailed view exhibits a width of 10 μm. (b) Comparison of two shadow masks. The one on the left was fabricated using ns laser pulses at a wavelength of 1064 nm, whereas the righthand one was made using ps laser pulses in the UV.

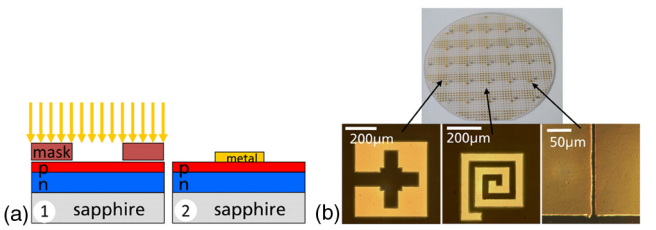

Fig. 6 (a) Schematics of the evaporation process. The shadow mask is placed on the planar wafer followed by the evaporation of the contact metallization. (b) LED wafer with Ni/Au p-contacts evaporated through a ps-laser fabricated shadow mask. A microscope image of one of these contacts is shown in the detailed view.

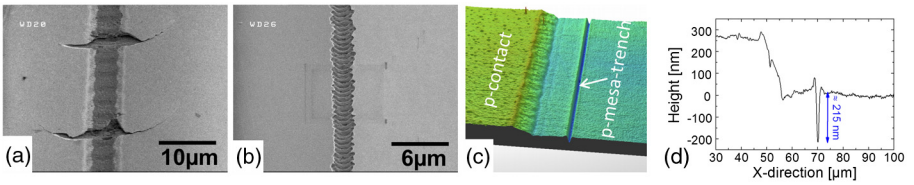

Fig. 7 (a) A p-mesa-trench fabricated with a focus diameter of 7 μm for electrical isolation. (b) A p-mesa-trench fabricated with a focus diameter of 1.7 μm. Due to the reduced pulse energy, the formation of cracks is avoided. (c) White light interferometer image of the p-mesa-trench fabricated at a distance of 15 μm away from the p-contact. (d) Depth profile across p-contact metal, p-GaN surface, and p-mesa-trench.

electrical isolation between the individual devices, and to expose the n-doped layer for the later deposition of the n-contact, mesa structures have to be formed. Usually this is done by photolithography and dry-etching techniques. In this study, the mesa structure is fabricated solely by laser direct writing techniques. Unlike standard lithography and etching-based mesa definition, here only a narrow trench is formed around the p-contact for electrical isolation, in the following called p-mesa-trench (Fig. 7). For the deposition of the n-contact, the width of the trench structure is not sufficient. Therefore a larger area has to be exposed in addition for n-contact deposition, as can be seen in Fig. 8.

Regarding these processing steps, the challenge is to stop laser ablation at a certain predefined depth. For the electrical isolation, it is necessary to cut through the p-GaN and active region layers until reaching the n-GaN, which is approximately 150 nm below the surface. Because the n-GaN has a thickness of around 1 μm, the intended depth for the p-mesa-trench has been set to around 230 nm, to allow for some variations in the actual ablation depth. This approach is similar to that taken for standard dry etching-based mesa fabrication. Preliminary experiments were carried out by just laser-drilling holes into the LED structure using multiple laser pulses and a pulse energy slightly above the ablation threshold. These experiments revealed that the ablation process is insensitive to the individual layers within the LED heterostructure.

For the ablation process, both focus diameters have been tested. Figure 7(a) shows an SEM-image of a p-mesa-trench fabricated using a focus diameter of 7 μm, an IPD of 4 μm, and a pulse energy of 0.65 μJ, resulting in a fluence of 1.69 J/cm^2. The intended depth of the laser-fabricated trench was achieved by a double-pass exposure to the focused laser beam. As can be seen in Fig. 7(a), the laser-processed trench suffers from cracking. By increasing the IPD, it was possible to avoid the cracking, but the resulting p-mesa-trench was too rough due to the large separation between the individual laser pulses. When decreasing the IPD, very deep cracking occurred, so ablation to a defined depth was not possible. When writing a straight line, the cracking appeared at fixed periodical intervals. Therefore the cracking is attributed to strain built up by each laser pulse. Due to accumulation effects, the strain is released by cracking occurring at a certain distance.

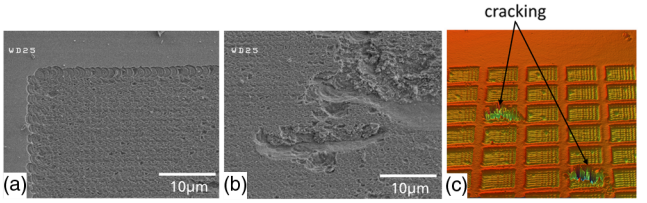

Fig. 8 (a) Exposed n-GaN area for the deposition of the n-contact. (b) Cracking of the n-GaN due to strain induced during the ablation process. (c) 15×8 μm^2 exposed n-GaN pads separated by a 3 μm spacing to stop the cracking process.

By reducing the focus diameter to 1.7 μm (second beam path of the laser-micromachining system), the pulse energy could be reduced by a factor of 17 while maintaining the same fluence. Because of the smaller focus diameter, the IPD could be reduced to 1 μm. A scanning electron microscope (SEM) image of a p-mesa-trench fabricated by double-pass exposure using the 1.7 μm laser focus can be seen in Fig. 7(b). Due to the smaller pulse energy strain is reduced and cracking is avoided when writing a line. Figure 7(c) shows a white-light interferometer image of the same p-mesa-trench fabricated at a distance of 15 μm from the p-contact. The cross-section through the structure shown in Fig. 7(d) reveals that the chosen parameter set results in an ablation depth of 215 nm. Due to the small focus diameter and the comparatively large IPD, the bottom of the p-mesa-trench depicts a roughness with a peak-to-valley variation of around 30 nm, which is still flat enough to ensure good electrical isolation. Reducing the IPD would again result in cracking of the epitaxial layers. The average ablation depth accuracy is around $\pm$30 nm, mainly dominated by the focus position with respect to the wafer surface, since the pulse-to-pulse stability for the chosen parameter set is around 2%.

To expose the n-GaN for the deposition of ohmic n-contact, the p-GaN and active region layers have to be removed on a larger area. Again the laser fluence was set to 1.69 J/cm^2 and the IPD was set to 1 μm in both x and y directions. Because of the overlap in x and y direction, a single-pass laser exposure was sufficient to expose the n-GaN. An SEM image of an exposed area can be seen in Fig. 8(a). Because of the pulse overlap in x and y direction, a larger strain is built up during the ablation process, resulting in cracking of the epitaxial layers at certain areas [Fig. 8(b)]. This is attributed to inhomogeneities in the epitaxial layers, probably caused by clustering of defects or dislocations. When such cracking occurs, it extends over very large distances, up to several millimeters. Therefore the scan strategy had to be optimized. Only small areas 15×8 μm^2 in size were exposed arranged in a 2-D array, with a grid of 3 μm wide strips left in between where no material was ablated. As can be seen from the white-light interferometer image in Fig. 8(c), the resulting small ridges are sufficient to stop cracking. For the contact metallization to be deposited onto the thus ablated surface, the conductivity of the n-GaN [50–100 $(\Omega\,\mathrm{cm})^{-1}$ (Ref. 14)] is large enough to ensure sufficient current spreading also into the unexposed strips. When no cracking occurs, the average ablation depth accuracy is

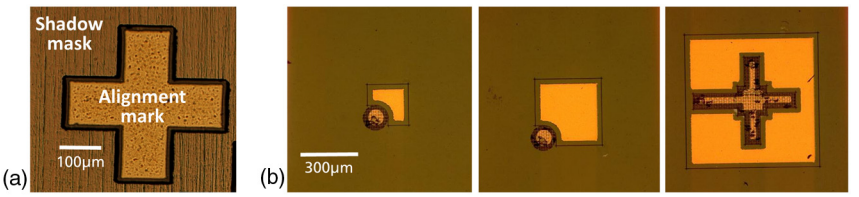

Fig. 9 (a) Microscope image of a shadow mask for the deposition of the n-contact metallization aligned on top of the structured LED wafer with the help of alignment marks. (b) Microscope image of different LEDs of various sizes and shapes, comprising p-contact, mesa patterning, and n-contact.

again around ±30 nm, whereas cracking results in deep craters in the micrometer range.

During the ablation process, gallium nitride is decomposed into Ga and N_2. Whereas the nitrogen is a volatile species at room temperature, liquid gallium remains as a residue in the p-mesa-trench. This can cause a short circuit between the p-GaN and n-GaN at the mesa sidewall. To remove the gallium deposit, an aqueous solution of 3% ammonia has been used followed by a KOH (3 mol) treatment. Both processes are carried out at room temperature. As a result, gallium is completely removed, whereas the LED structure remains unaffected. To minimize reverse bias leakage currents across the mesa sidewalls, an annealing step was introduced after the cleaning process, as will be discussed further in Sec. 5.2.

4.3 *n-Contact*

After exposing the n-GaN layer, ohmic n-contacts were deposited. For this purpose, again a ps UV laser fabricated shadow mask has been used. To allow a precise positioning of the n-contact mask relative to the p-contact metallization and mesa trenches, alignment marks have been incorporated in the shadow mask set, similar to those used in multiple-level photolithography mask sets. By using a mask aligner, the shadow mask used for the n-contact layer was aligned on top of the structured LED wafer [Fig. 9(a)]. A Ti/Al/Ni/Au metallization sequence was then evaporated as n-contact. A microscope image of different devices comprising the p-contact, a mesa structure, and an n-contact can be seen in Fig. 9(b). The distance between different features on the first- and second-level shadow masks has been set to 20 μm for these first devices, to make sure that no short circuit due to alignment errors occurs. It turned out that, due to the high precision achieved for the hole processing sequence, this distance could be reduced to 10 μm for future shadow mask sets. For comparison, for standard contact photolithography usually a distance of 2 μm is used as alignment tolerance. Due to the larger distance between the different features, the number of LEDs on a single wafer is reduced to approximately 80% compared to standard LED fabrication, but strongly depends on the device geometry.

4.4 *Trench Formation*

After deposition of the n-contact, the individual LED structures were isolated by trenches. In this processing step, all of the epitaxial layers are removed down to the sapphire substrate. As shown in Table 1, the ablation threshold of sapphire is significantly higher than that of GaN. Therefore the epitaxial layers can be removed by laser ablation as a self-limiting process without damaging the substrate.

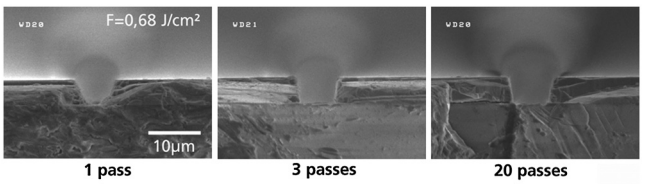

Fig. 10 SEM cross-section image of trenches fabricated in an LED structure, epitaxial grown onto sapphire substrate. Due to the self-limiting effect caused by the much higher ablation threshold of sapphire, the III-N epitaxial layers can be removed completely without damaging the sapphire.

To fabricate trenches between neighboring LED structures, the pulse energy was set to 0.68 J/cm^2 while the IPD was set to a small value of 100 nm. The results are shown in the SEM cross-section images in Fig. 10. When writing in single laser pass, all layers of the LED structure are almost completely removed. When increasing the number of laser passes to three, a clean and smooth bottom of the trench with steep sidewalls is formed. This shape is not changed when increasing the number of passes up to 20. Due to the higher ablation threshold of sapphire, laser ablation stops at the substrate. Therefore this process is less critical with respect to fluctuations in pulse energy, the IPD, or the focus position, compared to the fabrication of the p-mesa-trench and n-contact openings.

The subsequent dicing of the sapphire substrate can be carried out by conventional sawing and dicing techniques as well as by laser dicing, a processing technique already demonstrated for sapphire-based LEDs.[15]

5 Device Results

In the following, the electrical and optical characteristics of the laser-processed LEDs are presented. For a simple and fast measurement of multiple devices, the LEDs were measured on wafer without separation of the individual chips. Electrical contacting is realized by probe needles positioned onto the p- and n-contacts. To measure the optical output, the wafer is placed on top of an integrating sphere to collect the light emitted through the sapphire substrate. All measurements were carried out at room temperature.

5.1 *Electrical and Electroluminescence Characteristics*

The black solid curve in Fig. 11(a) shows the output power-vs.-current (P-I) characteristic of a 480 × 480 μm^2 square device with a p-contact area of around 0.165 mm^2. The light output power at 40 mA is 6.8 mW. The black solid curve in Fig. 11(b) shows the corresponding current-voltage (I-V) characteristic on a semi-logarithmic scale. Regarding the

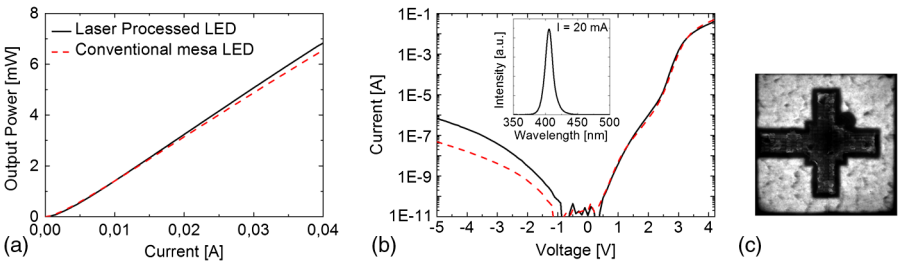

Fig. 11 (a) P-I characteristic of a laser-processed LED (solid black curve) and a conventional fabricated reference LED (dashed red curve). (b) Corresponding I-V characteristics of both devices. The inset shows the EL spectrum of the laser-processed LED. (c) EL image of the laser-processed LED at a drive current of 20 mA.

reverse bias current at −5 V, it can be seen that the device exhibits a leakage current of 680 nA corresponding to a current density of 4.1×10^{-4} A/cm^2. The reverse bias current is a useful indicator for residual leakage currents caused by defects in the epitaxial layers as well as by current leakage at the mesa side wall. The forward voltage at 20 mA is around 3.75 V. The inset in Fig. 11(b) shows the electroluminescence (EL) spectrum at a driving current of 20 mA. The emission wavelength is 406 nm. In Fig. 11(c), an EL image of the device at a driving current of 20 mA is displayed. It is the same device shown in the microscope image in Fig. 9(b) on the righthand side. The apparent granularity of the EL intensity pattern is correlated with the morphology of the epitaxial layer and not related to the laser processing.

5.2 *Comparison with Conventional Mesa LEDs*

When comparing the results of the laser processed LED to the P-I and I-V characteristics of a reference LED, fabricated using conventional photolithography combined with dry-etching and lift-off contact metal definition sharing the same epitaxial structure, these characteristics have been found to be similar. The red dashed curve in Fig. 11(a) shows the P-I characteristics of such a conventional fabricated reference LED. The optical output power at 40 mA is 6.5 mW, identical to that of the laser-processed LED within typical device-to-device and wafer-to-wafer scatter. Figure 11(b) shows a comparison of the corresponding I-V characteristics. When operating the LED in forward bias, the characteristics of the two devices are almost identical. The situation changes when operating the LEDs in reverse bias. Comparing the leakage current at −5 V, the current of the conventional mesa LED is 48 nA and thus more than an order of magnitude lower than that of the laser-processed LED. This finding strongly hints toward an increased sidewall current leakage for the laser-processed LED.

To exclude the possibility that the increased reverse bias leakage is caused by an enhanced defect density in the bulk of the p-n junction for the LED wafer, laser-processed and conventional dry-etched mesa LEDs were fabricated side by side on the same wafer. For that purpose, a third wafer was grown with the same epitaxial structure as the previous two wafers. In contrast to the processing sequence used above, a 15 nm titanium layer followed by a 100 nm nickel layer was evaporated through the shadow mask, which fulfills two tasks. First it serves as a p-contact as the previous metallization and second as an etching mask for dry etching. After the evaporation process, the wafer was divided into two parts. The p-mesa on the first half was again defined by patterning the epitaxial structure using the laser-micromachining system, whereas the mesa of the second half was defined using chemical dry etching also used for the fabrication of the conventional reference LED. Both samples were again cleaned in ammonia and KOH. After the p-mesa definition, devices from both parts of the wafer were analyzed with respect to their I-V characteristics. To get access to the n-GaN for electrical contacting, a small scratch was made at the periphery of each wafer half using a diamond tip. Then a small indium bump was pressed into each scratch, serving as an n-contact. Then the thus formed indium n-contact and the Ti/Ni p-contact were contacted by probe needles.

Figure 12(a) shows the resulting I-V characteristics of an LED containing the laser-machined p-mesa (black solid curve) and an LED containing the dry-etched p-mesa (blue solid curve). When operating the LEDs in forward bias, the characteristics are almost equal. But there is again a large difference when operating the LEDs in reverse bias, similar to the comparison in Fig. 11(b). At −5 V, the difference in leakage current is more than an order of magnitude.

Figure 12(b) shows the comparison of the reverse-bias leakage current at −5 V for the laser-machined p-mesa and the dry-etched p-mesa LEDs for different annealing temperatures. In contrast to the I-V characteristics in Fig. 12(a), each data point comprises the statistical average from a dataset taken on 13 different LEDs, to minimize device-to-device scattering. Without annealing the samples (20°C), the average leakage current of the laser-machined mesa is around an order of magnitude larger than that of dry-etched devices.

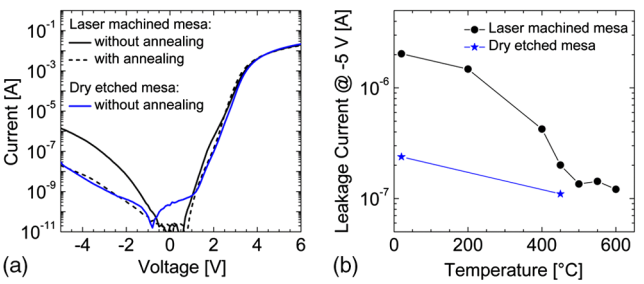

Fig. 12 (a) Comparison of the I-V characteristics for mesa LEDs fabricated side by side on the same wafer by laser p-mesa-trenching (black solid curve) and by dry etching (blue solid curve). After an annealing step, the characteristics of the laser machined mesa (black dotted curve) are almost equal to those of the dry-etched one. (b) Reverse-bias leakage current at −5 V for mesa-LEDs fabricated by laser trenching (black data points) and by dry etching (blue data points) as a function of post-processing annealing temperature for a fixed annealing time of 60 min. Statistical average over data recorded on 13 different LEDs of each variant are shown.

Because the devices were fabricated on the same wafer, variations of the leakage current through the bulk of the p-n junction are excluded in the following. Hence the difference in leakage current has to arise from the current flow on the mesa sidewall caused by the different p-mesa fabrication techniques. As can be seen in Fig. 12(b), the leakage current of the LEDs with the laser machined p-mesa can be reduced by a subsequent annealing step. The samples were annealed at different temperatures for 60 min in atmospheric oxygen, and the reverse-bias leakage current was then measured. As can be seen, the current can be reduced by an order of magnitude, reaching a constant value of about 130 nA for annealing temperatures at 500°C and above. This improvement is mainly attributed to the annealing of defects generated during the laser trenching on the sidewall of the p-mesa-trench. When annealing the reference sample fabricated by dry etching, only minor reduction in leakage current was observed. A slightly reduced leakage current of around 110 nA is achieved after annealing at 450°C, which is assumed to be dominated by the leakage current through the epitaxial layers. When comparing the I-V characteristics of the laser-machined p-mesa device after annealing (black dotted curve) and the dry-etched LED in Fig. 12(a), it can be seen that the characteristics are almost the same. This illustrates that after carrying out an appropriate annealing step, the laser processing has no adverse effect on the electrical properties of the LEDs.

6 Conclusion

We have successfully demonstrated the fabrication of GaN-based LEDs, only using UV ps laser-micromachining without any lithography steps. The fundamental process steps for the LED fabrication were demonstrated using laser-micromachining. Mesa trenches and n-contact openings were fabricated by direct laser processing, whereas "indirect" laser-machining-enabled processing steps using shadow masks were used for contact metal evaporation. The achieved output power, the forward voltage, and the leakage current are comparable to those of conventional reference LEDs with dry-etched mesas. Hence the present laser-based processing sequence has been proven to be a fast and flexible method for rapid prototyping of III-N LED devices featuring, for example, new chip layouts or different epitaxial structures.

References

1. M. Gower, "Industrial applications of laser micromachining," *Opt. Express* **7**(2), 56–67 (2000).
2. F. G. Bachmann, "Industrial laser application," *Appl. Surf. Sci.* **46**(1–4), 254–263 (1990).
3. R. R. Gattass and E. Mazur, "Femtosecond laser micromachining in transparent materials," *Nat. Photonics* **2**(4), 219–225 (2008).
4. C. B. Schaffer, A. Brodeur, and E. Mazur, "Laser-induced breakdown and damage in bulk transparent materials induced by tightly focused femtosecond laser pulses," *Meas. Sci. Tech.* **12**(11), 1784–1794 (2001).
5. B. N. Chichkov et al., "Femtosecond, picosecond and nanosecond laser ablation of solids," *Appl. Phys. A Mater. Sci. Process.* **63**(2), 109–115 (1996).
6. G. Heise et al., "Monolithical serial interconnects of large CIS solar cells with picosecond laser pulses," *Phys. Proced.* **12**(Pt. B), 149–155 (2011).
7. G. Raciukaitis and P. Gecys, "Picosecond-laser structuring of thin films for CIGS solar cells," *J. Laser Micro/Nanoeng.* **5**(1), 10–15 (2010).
8. R. Murison et al., "CIGS P1, P2, and P3 laser scribing with an innovative fiber laser," in *Proc. 35th IEEE PVSC*, Honolulu, Hawaii, June 20–25 (2010).
9. Y. Jee, M. F. Becker, and R. M. Walser, "Laser-induced damage on single-crystal metal surface," *J. Opt. Soc. Am. B* **5**(3), 648–659 (1988).
10. D. Ashkenasi et al., "Surface damage threshold and structuring of dielectrics using femtosecond laser pulses: the role of incubation," *Appl. Surf. Sci.* **150**(1–4), 101–106 (1999).
11. M. Hörstmann-Jungemann, "3D-microstructuring of sapphire using fs-laser irradiation and selective etching," *J. Laser Micro/Nanoeng.* **5**(2), 145–149 (2010).
12. H. Shibata et al., "High thermal conductivity of gallium nitride (GaN) crystals grown by HVPE process," *Mater. Transact.* **48**(10), 2782–2786 (2007).
13. G. Y. Mak, E. Y. Lam, and H. W. Choi, "Deep etch of GaN by laser micromachining," *Phys. Stat. Solidi (C)* **7**(7–8), 2151–2153 (2010).
14. Y. Oshima et al., "Thermal and electrical properties of high-quality freestanding GaN wafers with high carrier concentration," *Phys. Stat. Solidi (C)* **4**(7), 2215–2218 (2007).
15. Yole Développement, "LED manufacturing – technologies & costs," http://apps1.eere.energy.gov/buildings/publications/pdfs/ssl/perkins_fairfax09.pdf, DOE Workshop April 2009 (7 August 2012).

Biographies and photographs of the authors are not available.